Broadband Small-Aperture High-Gain Ridge Horn Antenna Array Element

Laila Marzall, *Student Member, IEEE,* Paige Danielson, *Student Member, IEEE,* Gregor Lasser, *Member, IEEE,* and Zoya Popović, *Fellow, IEEE*

***Abstract*—This paper presents the design and characterization of an octave-bandwidth, small-aperture, linearly-polarized, high-gain horn antenna operating in the 6-12 GHz band for active arrays. The aperture size is limited by the waveguide feed cutoff at lower frequencies, and by grating lobes at higher frequencies. The radiating structure is composed of an E-plane flared horn with an exponential double ridge fed by a low-loss waveguide-to-microstrip transition, eliminating the need for additional connections between the antenna elements and the beamforming and amplification circuits. The horn is loaded with an artificial dielectric with $1 < \epsilon_{r,\mathrm{eff}} < 2.2$, which lowers the cutoff frequency and improves phase distribution over the aperture. The lens and feed loading structure are designed together to improve matching without degrading the radiation pattern. A prototype is fabricated in brass using split-block machining, and the lens is machined from 16 parallel dielectric slabs. The measured performance is in agreement with simulations.**

***Index Terms*—Broadband horns, dielectric-loaded apertures, lens antennas, microstrip-to-waveguide transition.**

I. Introduction

BROADBAND ANTENNA ARRAYS that cover octave bandwidths require element design that takes into account the element-to-element spacing at the highest frequency of interest. Traditional elements such as Vivaldi endfire slots can cover large bandwidths (>5:1), e.g. [1], while ridge horns have higher power handling but typically cover less bandwidth (>2:1, e.g. [2]). A 4-10 GHz open ridge waveguide array is presented in [3], and an X-band dual-polarized open-ended ridge waveguide monopulse array is shown in [4]. Millimeter-wave circular corrugated horn arrays with greater than octave bandwidths from 120-270 GHz and 80-180 GHz are demonstrated in [5].

The physical aperture size of a ridge horn element in an array is a tradeoff between bandwidth due to cuttoff frequency at the lower end, and grating lobe appearance at the higher frequency end. In this paper, we show a design of a small double-ridge exponentially-flared 6-12 GHz horn with dielectric loading, shown in Fig.1. The antenna element is designed to enable straightforward integration with active transmit/receive components, with a feed that includes a low-loss double-ridge waveguide-to-microstrip transition [6]. The aperture is a square of size $a = 21.27$ mm, which is about $\lambda_0/2$ at the lower edge of the band and λ_0 at the upper edge. The horn is loaded with an artificial dielectric with $1 < \epsilon_r < 2.2$, which lowers the horn cutoff frequency. The lens is integrated with the feed loading structure to improve matching while not degrading the radiation pattern across the band.

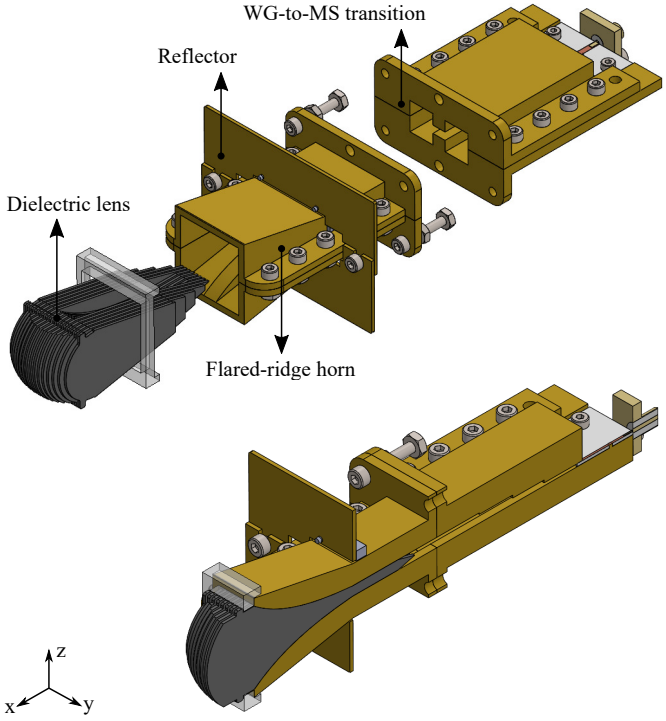

Figure 1. Double-ridge horn antenna with waveguide-to-microstrip transition. The top image shows the exploded view with SMA connector and microstrip 50-Ω line, transition to double-ridge waveguide, flared horn and dielectric lens and loading, consisting of 16 dielectric slabs. The bottom figure shows the xz cross-section. All metal parts are made of brass while the dielectric slabs are 0.762 mm thick with $\epsilon_r = 2.2$.

Figure 1 shows the main parts of the single linearly-polarized antenna element. A cross-sectional view in the xz-plane describes the final assembly with transition, flare and lens details. A prototype is fabricated in brass using split-block machining, and the lens is machined from 16 parallel dielectric slabs. The measurements are performed with the integrated microstrip transition.

The paper is organized as follows. Section II describes the design of the double-ridge waveguide feed and air-filled horn, motivating the need for improving the performance of the horn as an array element. Section III discusses how introducing an exponential taper, dielectric loading in the feed, and addition

The authors are with the Department of Electrical, Computer and Energy Engineering, University of Colorado, Boulder, CO, 80309 USA e-mails: laila.marzall@colorado.edu and zoya@colorado.edu

This work was supported by Office of Naval Research, award number N00014-19-1-2487. L. Marzall thanks partial support through a CAPES fellowship award number 88881.171772/2018-01. P. Danielson thanks the Department of Defense (DoD) for funding through the National Defense Science Engineering Graduate (NDSEG) Fellowship.

of a dielectric lens improve the element gain and match. The final design includes integration with a wideband microstrip-to-waveguide transition [6]. Section IV presents the fabrication and measurement results of the antenna at the SMA connector reference plane.

II. Ridge Waveguide Feed and Air-Filled Horn

The design starts with the waveguide feed selection. Next, the limitations of an air-filled linearly flared horn related to the lower-frequency limit are discussed, leading to the design approach and final geometry described in Section III.

A. Double Ridge-Waveguide Feed Design

Rectangular waveguides do not cover an octave, resulting in a choice of a ridge waveguide feed which reduces the fundamental mode cutoff frequency. Single, double and quad ridge waveguides have all been shown to increase bandwidth, e.g. [7] [8]. A double-ridge waveguide was chosen as a tradeoff between complexity and radiation pattern symmetry of the horn. Fig.2 shows the results of a parameter study for a given waveguide size ($a_{\rm wg}, b_{\rm wg}$), where the two symmetrical ridge widths and heights are varied. From the plot, $w_{\rm rg} = 4.47\,$mm and $h_{\rm rg} = 3.63\,$mm are manufacturable and result in the largest ratio of the lower cutoff frequency to the frequency where the next higher order mode starts propagating.

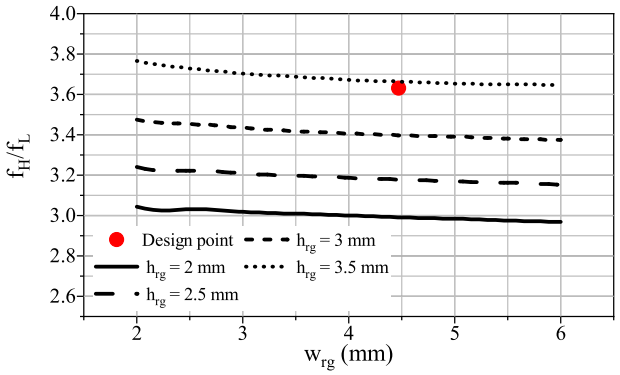

Figure 2. Ratio of upper to lower frequency cutoff for a double-ridge waveguide with sides $a_{\rm wg} = 21.27\,$mm and $b_{\rm wg} = 9.9\,$mm, as a function of ridge height $h_{\rm rg}$ for several ridge widths $w_{\rm rg}$.

As a starting point, the feed is flared with a linear ridge taper for a compact air-filed horn element. An air-filled horn will have a reduced bandwidth compared to the feed itself, following the reasoning in [9] for a standard rectangular waveguide. This can be understood from the dominant-mode impedance and normalized guided wavelength for this specific double-ridge design, shown in Fig. 3, as simulated using *Ansys HFSS*. The dispersive wave impedance, which varies from 160-120 Ω in the 6-12 GHz range, leads to the first design constraint. Namely, the horn has to match this waveguide impedance to the constant 377-Ω free-space impedance. The second constraint can be inferred from the normalized guided wavelength (dashed line in Fig.3).A well-matched antenna requires reducing the guided wavelength in the lower part of the band to maintain a constant normalized propagation constant, and therefore a constant delay.

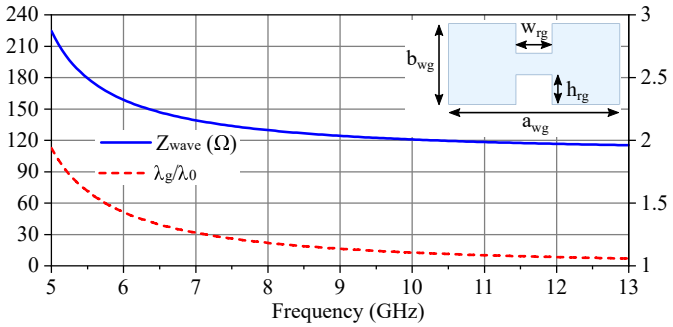

Figure 3. Simulated air-filled ridge waveguide wave impedance and normalized guided wavelength ($\lambda_{\rm g}/\lambda_0$) used for the design. Dimensions are $a_{\rm wg} = 21.27$, $b_{\rm wg} = 9.9$, $w_{\rm rg} = 4.47$, and $h_{\rm rg} = 3.63\,$mm. The wave impedance is calculated by integrating the transverse electric field of the fundamental mode to find the voltage ($Z_{\rm wave} = V^2/P$).

B. Air-Filled Linear-Tapered Ridge Horn

The feed from Fig.3 is next flared with a linear taper. To understand the performance limitations of a small-aperture air-filled horn, we plot the reflection coefficient as a function of the horn length h for a constant square aperture size of $a = 21.27\,$mm. Fig. 4 shows the de-embedded reflection coefficient from port $\rm P_1$ to port $\rm P_2$ when loaded with an air-filled, E-Plane flared horn, for various values of horn height h. One can observe that the cut-off frequency does not significantly vary with changes in the horn length, and we address this in the next section.

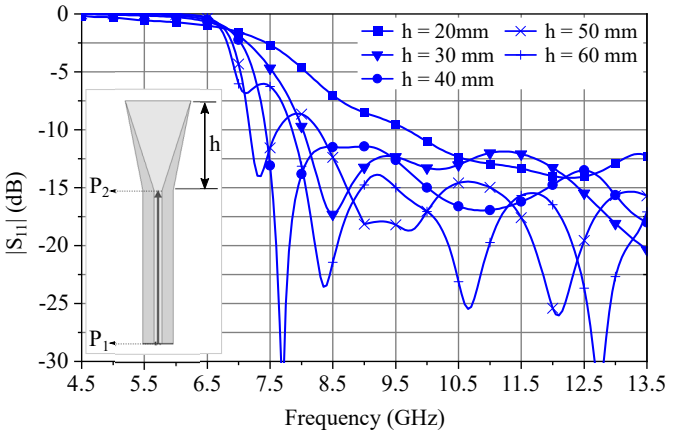

Figure 4. Reflection coefficient magnitude at waveguide feed ($\rm P_2$) for different horn lengths, while maintaining square aperture size $a = 21.27\,$mm. The simulations are de-embedded from $\rm P_1$ to $\rm P_2$. The waveguide feed length is 50 mm.

III. Exponentially-Flared Dielectric-Loaded Small-Aperture Horn

To improve both the matching at the lower end, we introduce dielectric loading in the feed, extended to a dielectric lens loading of the horn. Aperture efficiency enhancement of small horns by Teflon loading is shown in [10], with an application to limited scan-angle arrays. Dielectric loading of circular and rectangular horns is also discussed in [11] and [12] for improving radiation patterns. In [13], it is shown that dielectric loading can improve the reflection coefficient of a horn array. A short horn using low-loss anisotropic meta-material transverse loading is shown to improve gain in [14].

This article has been accepted for publication in a future issue of this journal, but has not been fully edited. Content may change prior to final publication. Citation information: DOI 10.1109/LAWP.2021.3060779, IEEE Antennas and Wireless Propagation Letters

In order to improve the match at the waveguide feed, an exponential taper of the ridge is introduced, with a final profile obtained with *Ansys HFSS* simulations, shown in Fig.5a, while Fig.5b shows details of a dielectric lens that completely fills the taper. The dielectric lens is implemented with 16 parallel dielectric slabs with $\epsilon_r = 2.2$, 0.762-mm thick, and spaced 0.55 mm apart. To understand how the taper, dielectric filling of the feed and the dielectric lens impact antenna performance, we next show the evolution of the design that achieves an improvement in impedance bandwidth at the lower frequency end without radiation pattern degradation.

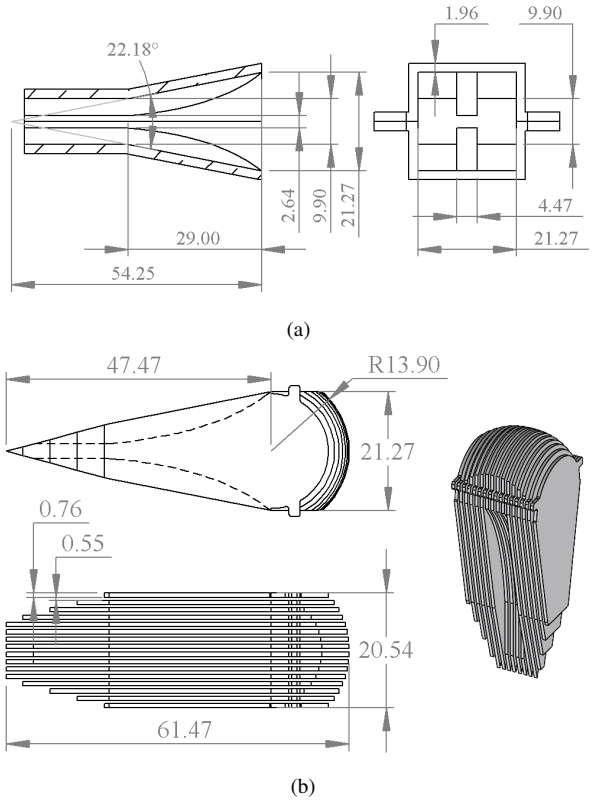

Figure 5. (a) Exponentially-tapered horn dimensions, shown with a cross-section in the xz and yz cuts. The aperture size is 21.27 mm, corresponding to $0.425\,\lambda_0$, $0.638\,\lambda_0$, and $0.851\,\lambda_0$ at $f_0 = 6, 9, 12$ GHz, respectively. (b) Geometry of the lens which completely fills the taper and consists of 16 dielectric slabs, with dimensions given in mm.

Fig.6 gives a comparison between the air-filled linear (solid black line) and exponential (dashed line) tapers, showing an improved match at the lower frequency end. Further improvement is obtained with a solid dielectric filling with a flat aperture surface. Because this antenna element is designed for an active transmit array, a design that allows air flow is preferable. This is obtained by replacing the solid dielectric with 16 parallel dielectric slabs with $\epsilon_r = 2.2$, 0.762-mm thick, spaced 0.55 mm apart. As shown in Fig.6, these two designs show very similar performance in return loss (dotted lines). Finally, instead of a planar aperture, the dielectric slabs are extended to form a lens (Fig.1, and this further improves the match across the band (red line in Fig.6). Normalized H-plane radiation patterns in Fig.7 compare the first and final designs at 6 and 12 GHz. At the lower frequencies, performance was improved in the final design due to the better matching from the addition of the loading and lens. At the higher frequencies, there was also an increase in gain as large as 1.7 dB at 9 GHz.

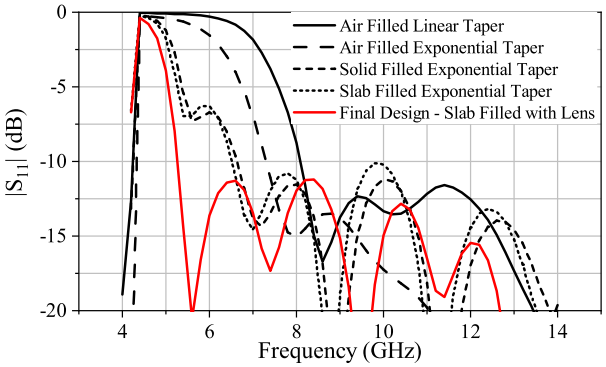

Figure 6. Comparing $|S_{11}|$ for each of the design steps starting with a linearly flared air filled horn, then adding an exponential flare, adding a solid dielectric filling ($\epsilon_r = 1.6$), changing the filling to slabs with $\epsilon_r = 2.2$, and finally adding a dielectric lens. Each step in the design improves the match across the band, and especially at the lower end of the frequency range.

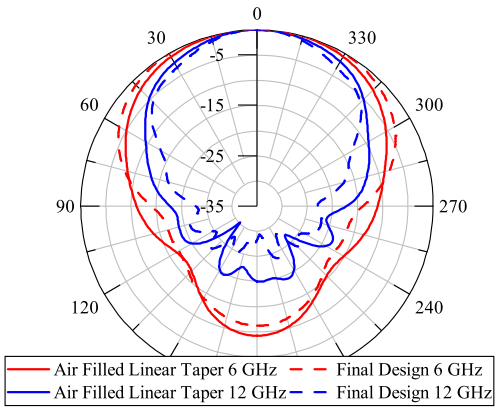

Figure 7. The H-plane radiation pattern at 6 GHz and 12 GHz for the linear air filled horn compared to the final design with dielectric loading and lens.

For integration with an active array, a transition to microstrip is designed as detailed in [6], with geometry shown in Fig.8. When this transition is simulated together with the waveguide feed and dielectric-filled horn, the VSWR=2 bandwidth is from 5.2 to 12.7 GHz, as shown in Fig.9. Note that the increased back radiation at the lowest frequency in the E plane around 250° is expected based on the results in [6], and is due to the open microstrip transition.

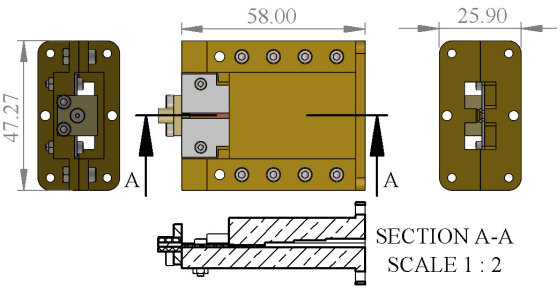

Figure 8. Geometry of the microstrip to singe-ridge waveguide transition described in detail in [6]. The dimensions are given in mm.

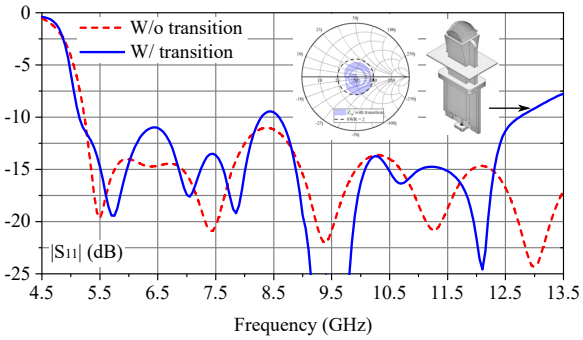

Figure 9. Simulated $|S_{11}|$ over bandwidth of horn with (solid) and without (dashed) coaxial-to-microstrip-to-waveguide transition. The degradation above 12.5 GHz is due to the coaxial-to-microstrip transition mismatch.

IV. Fabrication and Measurements

The antenna is fabricated from brass using split-block machining in several elements connected with flanges, as shown in Fig.1. The dielectric lens is made of 16 Rogers' Duroid 0.762-mm thick dielectric slabs milled to the designed shape. A 3D printed frame is fabricated to hold the dielectrics. The measured reflection coefficient of two prototypes is shown in Fig.10 to quantify the repeatibility of the fabrication process. As expected, the variability is more pronounced at higher frequencies, but the measured input reflection coefficient is below -9 dB over the entire range for both prototypes, following the simulated performance. The gain, presented in Fig.10, was measured in a non-commercial anechoic chamber, using the two prototypes and assuming the gains are the same. A photograph of one of the prototypes is shown in the inset. In the measurement setup, the feed cable is in the 180° direction, contributing to reflections and errors in the back lobe data, which is seen e.g. in the 6-GHz measured patterns at that angle. The measured radiation patterns compared to simulated ones are shown in Fig.11.

V. Conclusion

This paper presents the design and implementation of a small octave-bandwidth single linearly-polarized horn antenna, suitable for array integration. The element size is $0.5\lambda_0$ at the lower edge of the octave band, so higher inter-element coupling is expected, affecting the active scan reflection coefficient. On the other hand, grating lobes are expected when scanning at frequencies in the upper part of the band. A comparison with horn antennas with similar bandwidths in Table I shows that we are achieving comparable gain across an octave with a $0.56\lambda_0^2$ aperture at the center frequency. The feed is implemented in ridge waveguide and includes a transition to a 50-Ω microstrip line, allowing direct integration with active circuits with a common thermal and RF ground. A dielectric-slab lens extends the lower-frequency impedance matched region without significantly affecting the radiation pattern.

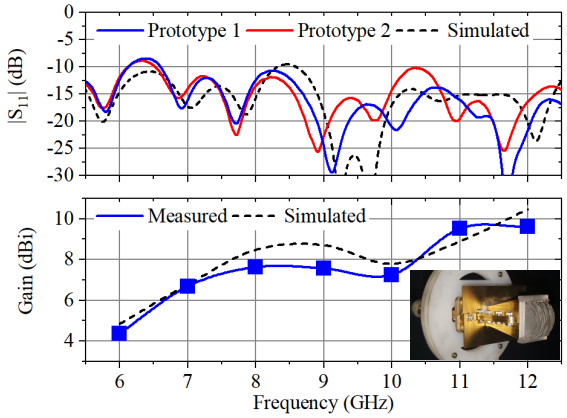

Figure 10. Measured and simulated $|S_{11}|$ (top) and gain (bottom).

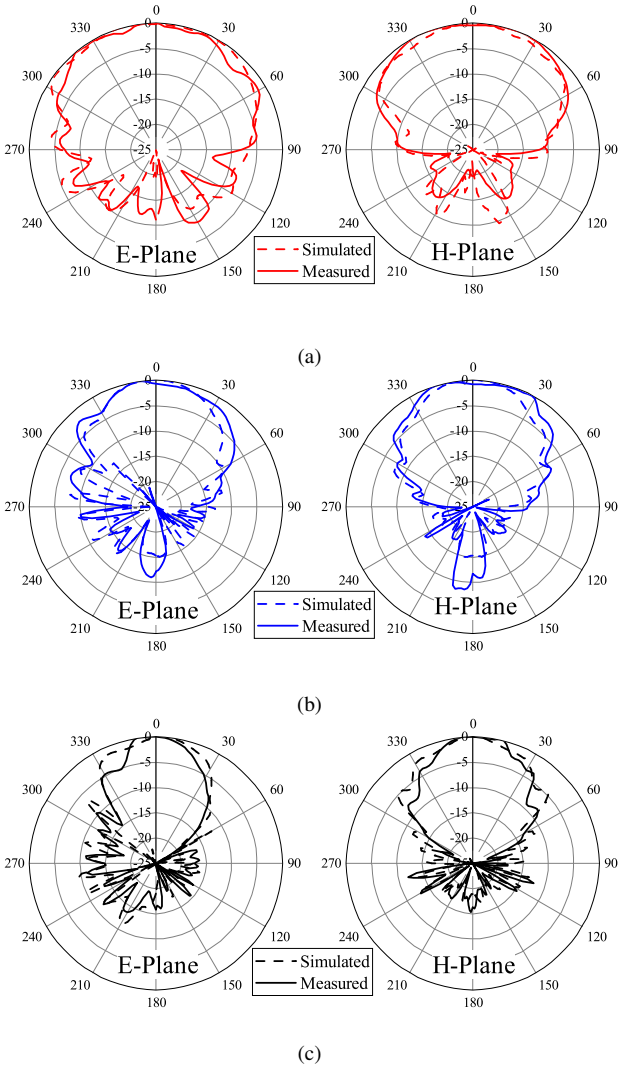

Figure 11. Measured (solid) and simulated (dashed) E- and H-plane radiation patterns at (a) 6 GHz, (b) 9 GHz, and (c) 12 GHz.

Table I
Comparison with Similar Horns

Ref	Type	BW (GHz)	Aperture (λ_0^2)	Gain (dBi)
[4]	Open-ended WG	8 - 12	0.54	9.7 - 14
[15]	Horn fed by dipole array	1.5 - 4.5	8.9	11 - 20
[16]	Dielectric-loaded horn	8 - 16	29, conical	n/a
[17]	Metamaterial-loaded	3.7 - 7	7.28	16 - 24
[18]	3D-printed horn array	29 - 37	0.5	8
This work	Ridge waveguide, dielectric-loaded horn	6 - 12	0.56	5 - 10

REFERENCES

[1] D. H. Schaubert, S. Kasturi, A. O. Boryssenko, and W. M. Elsallal, "Vivaldi antenna arrays for wide bandwidth and electronic scanning," in *The Second European Conference on Antennas and Propagation, EuCAP 2007*, 2007, pp. 1–6.

[2] G. Laughlin, E. Byron, and T. Cheston, "Very wide-band phased-array antenna," *IEEE Transactions on Antennas and Propagation*, vol. 20, no. 6, pp. 699–704, 1972.

[3] F. F. Dubrovka, S. Y. Martyniuk, D. O. Vasylenko, and O. Postulga, "Ultrawideband tapered slot, waveguide and dipole antenna arrays," in *2017 XI International Conference on Antenna Theory and Techniques (ICATT)*. IEEE, 2017, pp. 20–25.

[4] J. S. Kim, D. W. Woo, and R.-C. Jeong, "Dual-polarized open-ended waveguide with squinted beam for x-band monopulse antenna on a small diameter cylinder," in *2018 IEEE International Symposium on Antennas and Propagation & USNC/URSI National Radio Science Meeting*. IEEE, 2018, pp. 523–524.

[5] J. Shi, S. Weinreb, W. Zhong, X. Yin, and M. Yang, "Quadruple-ridged flared horn operating from 8 to 50 ghz," *IEEE Transactions on Antennas and Propagation*, vol. 65, no. 12, pp. 7322–7327, 2017.

[6] J. R. Montejo-Garai, L. Marzall, and Z. Popović, "Octave bandwidth high-performance microstrip-to-double-ridge-waveguide transition," *IEEE Microwave and Wireless Components Letters*, 2020.

[7] S. Hopfer, "The design of ridged waveguides," *IRE Transactions on Microwave Theory and Techniques*, vol. 3, no. 5, pp. 20–29, 1955.

[8] W. Sun and C. A. Balanis, "Analysis and design of quadruple-ridged waveguides," *IEEE Transactions on Microwave Theory and Techniques*, vol. 42, no. 12, pp. 2201–2207, 1994.

[9] A. Yaghjian, "Approximate formulas for the far field and gain of open-ended rectangular waveguide," *IEEE Transactions on Antennas and Propagation*, vol. 32, no. 4, pp. 378–384, 1984.

[10] G. Tsandoulas and W. Fitzgerald, "Aperture efficiency enhancement in dielectrically loaded horns," *IEEE Transactions on Antennas and Propagation*, vol. 20, no. 1, pp. 69–74, 1972.

[11] J. James, "Engineering approach to the design of tapered dielectric-rod and horn antennas," *Radio and Electronic Engineer*, vol. 42, no. 6, pp. 251–259, 1972.

[12] M. Hamid, "Dielectric loaded horn antennas having improved radiation characteristics," May 8 1984, uS Patent 4,447,811.

[13] S. P. Skobelev and A. Yaparova, "Modeling of horn array antennas with protruding dielectric elements," in *2007 6th International Conference on Antenna Theory and Techniques*. IEEE, 2007, pp. 409–411.

[14] Y. He, N. Ding, L. Zhang, W. Zhang, and B. Du, "Short-length and high-aperture-efficiency horn antenna using low-loss bulk anisotropic metamaterial," *IEEE Antennas and Wireless Propagation Letters*, vol. 14, pp. 1642–1645, 2015.

[15] W. F. Moulder, K. Sertel, and J. L. Volakis, "Compact ultrawideband beam-steering horn antenna," in *Proceedings of the 2012 IEEE International Symposium on Antennas and Propagation*. IEEE, 2012, pp. 1–2.

[16] A. D. Olver, P. J. B. Clarricoats, and K. Raghavan, "Dielectric cone loaded horn antennas," *IEE Proceedings H - Microwaves, Antennas and Propagation*, vol. 135, no. 3, pp. 158–162, 1988.

[17] C. P. Scarborough, Q. Wu, D. H. Werner, E. Lier, R. K. Shaw, and B. G. Martin, "Demonstration of an octave-bandwidth negligible-loss metamaterial horn antenna for satellite applications," *IEEE Transactions on Antennas and Propagation*, vol. 61, no. 3, pp. 1081–1088, 2013.

[18] Y. Li, L. Ge, J. Wang, S. Da, D. Cao, J. Wang, and Y. Liu, "3-d printed high-gain wideband waveguide fed horn antenna arrays for millimeter-wave applications," *IEEE Transactions on Antennas and Propagation*, vol. 67, no. 5, pp. 2868–2877, 2019.